Accepted Manuscript

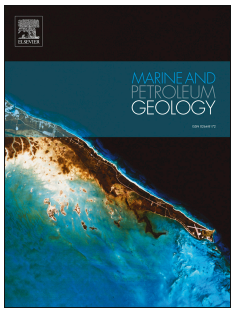

Formation of tubular carbonate conduits at Athina mud volcano, eastern Mediterranean Sea

Leonardo Tamborrino, Tobias Himmler, Marcus Elvert, Stefano Conti, Alessandro F. Gualtieri, Daniela Fontana, Gerhard Bohrmann

PII: S0264-8172(19)30200-4

DOI: https://doi.org/10.1016/j.marpetgeo.2019.05.003

Reference: JMPG 3823

To appear in: *Marine and Petroleum Geology*

Received Date: 9 August 2018

Revised Date: 30 April 2019

Accepted Date: 3 May 2019

Please cite this article as: Tamborrino, L., Himmler, T., Elvert, M., Conti, S., Gualtieri, A.F., Fontana, D., Bohrmann, G., Formation of tubular carbonate conduits at Athina mud volcano, eastern Mediterranean Sea, *Marine and Petroleum Geology* (2019), doi: https://doi.org/10.1016/j.marpetgeo.2019.05.003.

Formation of tubular carbonate conduits at Athina mud volcano, eastern Mediterranean Sea

Leonardo Tamborrino[a, b, *], Tobias Himmler[b †], Marcus Elvert[b], Stefano Conti[a], Alessandro F. Gualtieri[a], Daniela Fontana[a], Gerhard Bohrmann[b]

[a] Dipartimento di Scienze Chimiche e Geologiche, Università di Modena e Reggio Emilia, Via Campi 103, 41125 Modena, Italy

[b] MARUM- Center for Marine Environmental Sciences and Department of Geosciences, University of Bremen, Leobenerstrasse 8, 28359 Bremen, Germany

[†] Present address: Geological Survey of Norway, Post box 6315 Torgard, 7491 Trondheim, Norway

*Corresponding author, Phone number: +49 421218 – 65849 Mail: ltamborrino@marum.de

Highlights

- Carbonate conduits are composed of authigenic ^{13}C-depleted Mg-calcite and aragonite
- Lipid biomarkers reveal involvement of AOM consortia in carbonate precipitation
- AOM-induced early lithification of burrows forms tubular carbonate conduits

Abstract

Tubular carbonate conduits (TCC) represent the termination of fluid plumbing systems in environments of hydrocarbon seepage and play a relevant role in the discharge of methane from sub-seafloor sediments to the water column. However, the biogeochemical reactions and biological activities involved in their formation are not fully understood. To address this, TCC samples were collected with a remotely operated vehicle from the seabed on the SW flank of the Athina mud volcano in the eastern Mediterranean Sea. Petrographic, mineralogical, stable carbon and oxygen isotope and lipid biomarker analyses were performed to elucidate the formation processes of the tubular carbonates. Clotted and fibrous aragonite form the internal lining of the cavities, while the outer portion of the tubes is formed by micritic Mg-calcite cementing hemipelagic sediment. ^{13}C-depleted Mg-calcite and aragonite (as low as –14.4 ‰ V-PDB) and lipid biomarkers (archaeol, –89.8 ‰ V-PDB) indicate that carbonate precipitation was influenced by sulfate-

dependent anaerobic oxidation of methane (AOM). AOM locally enhances aragonite precipitation, thereby facilitating early lithification of the conduits within the mud volcano sediments. The size and morphology of the TCC comparable with the buried portion of tubeworm colonies found in the proximity of the sampling site. However, our results suggest that TCC likely formed by the action of burrowing organism rather than being mineralizations of the tubeworm colonies. This study provides new insights into the interpretation and understanding of TCC, highlighting the role of macrofaunal activity in the formation of migration pathways for hydrocarbon-rich fluids on the flank of a mud volcano.

.

Keywords: authigenic minerals, lipid biomarkers, fluid conduits, hydrocarbon seeps, mud volcanoes, Anaximander Mountains

Abbreviations

TCC, tubular carbonate conduits. MV, mud volcano. AOM, anaerobic oxidation of methane. SRB, sulfate-reducing bacteria. ANME, anaerobic methanotrophic archaea. XRD, x-ray diffraction. ROV, remote operated vehicle. AUV, autonomous underwater vehicle. GC-MS, gas chromatography-mass spectrometer. GC-IRMS, GC-isotope ratio MS. HPLC-MS, high performance liquid chromatography MS. TMS, trimethylsilyl. FAMEs, fatty acid methyl esters. cfA, clotted and fibrous aragonite. M, micritic Mg-calcite. Di, late detrital infilling. V-PDB, Vienna Pee Dee Belemnite. DIC, dissolved inorganic carbon. TLE, total lipid extracts. GDGT, glycerol dialkyl glycerol tetraethers. DAGE, dialkyl glycerol ether. PMI, 2,6,10,15,19-pentamethyleicosane. Bp, biphytane. Bp-Cren, crenarchaeol-derived biphytane. FA, fatty acid. ai, methyl-branching at ante-iso position (ω3). MI, methane index.

Introduction

Mud volcanoes provide pathways for the expulsion of different types of over-pressured deep-seated hydrocarbon-enriched fluids and sediments (Milkov et al., 2003; Kopf, 2002; Dimitrov, 2002). In the eastern Mediterranean Sea, numerous methane seeps are associated with mud volcanoes (e.g., Aloisi et al., 2000; Charlou et al., 2003; Olu-Le Roy et al., 2004; Pape et al., 2010). The sulfate-dependent anaerobic oxidation of methane (AOM; e.g. Hoehler et al., 1994) forms the basis for higher benthic chemosynthetic communities

54 at methane seeps. In most of the AOM sites studied, anaerobic methanotrophic archaea (ANME) co-occur
55 with sulfate-reducing bacteria (SRB), suggesting that AOM is mediated according to the following equation
56 (Boetius et al., 2000; Orphan et al., 2001):

$$CH_4 + SO_4^{2-} \rightarrow HCO_3^- + HS^- + H_2O$$

57 The reaction product hydrogen sulfide sustains sulfide-oxidizing bacteria, frequently occurring at seeps as
58 free-living bacterial mats or as endosymbionts of the macrofaunal seep-related species (Sahling et al., 2002)
59 such as tubeworms (Sibuet and Olu, 1998; Levin, 2005). AOM-produced bicarbonate increases the pore
60 water alkalinity and thus induces the precipitation of authigenic carbonates which are ^{13}C-depleted based on
61 the stable carbon isotope nature of methane consumed (Aloisi et al., 2000; Peckmann et al., 2001; Bahr et al.,
62 2009; Himmler et al., 2015). Correspondingly, the biomass of AOM consortia is likewise characterized by
63 strongly negative $\delta^{13}C$ values of specific lipid biomarkers, corroborating assimilation of methane-derived
64 carbon (e.g. Hinrichs et al., 2000; Elvert et al., 1999, 2000). AOM lipid biomarkers are preserved in
65 authigenic seep-carbonates, revealing further details on the biogeochemical processes during carbonate
66 precipitation (e.g. Thiel et al., 1999; Pancost et al., 2000; Peckmann and Thiel, 2004; Birgel et al., 2008).
67 Authigenic seep-carbonates have been described in modern and fossil seep-deposits with different
68 morphology and texture, including tubular conduits, slabs, crusts, chemoherms, breccias and stromatolites
69 (Bohrmann and Greinert, 1998; Michaelis et al., 2002; Campbell, 2006; De Boever et al., 2009; Bayon et al.,
70 2013; Conti et al., 2014; Zwicker et al., 2015; Himmler et al., 2018; Argentino et al., 2019). Whereas
71 chemoherms and stromatolites are associated with AOM-activity at or above the sediment-water interface
72 under oxygen-deprived bottom water conditions (e.g. Michaelis et al., 2002; Bayon et al., 2013; Himmler et
73 al., 2018), breccias and tubular carbonate conduits (TCC) are typical of sub-seabed formation conditions (De
74 Boever et al., 2006; Nyman et al., 2010; Conti et al., 2014; Zwicker et al., 2015).
75 The aim of this study is to assess the formation conditions of TCC from the Athina MV in the eastern
76 Mediterranean Sea (Fig. 1). We combined seafloor observations with a set of data collected from the
77 subsamples of a main specimen TCC (size, morphology, petrography, mineralogy, stable isotopes, and lipid
78 biomarkers) to discuss the two main possible processes for TCC formation: (1) activities of burrowing
79 organisms and (2) mineralization of tubeworm conduits. The results highlight a relevant role of AOM in the

formation of TCC and provide insights to discern features and details related to their origin, which contribute to the understanding of processes during fluid migration at hydrocarbon seeps associated with MVs.

Geological setting

Athina MV is situated in the eastern Mediterranean Sea, at the junction of the Hellenic and the Cyprus Arcs (Fig. 1A; ten Veen et al., 2004). Three main seamounts, Anaximander s.s., Anaxagoras and Anaximenes, compose the Anaximander Mountains (Zitter et al., 2006). Numerous MVs are associated with Anaximander Mountains, including the Athina MV, which occurs on the SE flank of the Anaximenes.

Since the Miocene, the Anaximander Mountains have experienced an intense tectonic activity, recently expressed by strike-slip faulting with transtensional stresses (Aksu et al., 2009),controlling the distribution and activity of MVs in the Anaximander Mountains (Zitter et al., 2006). The seepage associated to the Anaximander Mountains MVs is sustained by thermogenic hydrocarbon, migrated upwards during the tectonically-driven formation of the MVs (Pape et al., 2010).

Athina MV forms a circular structure on the slope of the Anaximenes seamount at around 1780 m water depth. An AUV-derived bathymetry shows that most of the mud flows were directed downslope to the southeast (Fig. 1B). Separated rims identify some of the youngest generations of mud flows, propagating from the emission spot near NE peak, where gas hydrates have been sampled (Bohrmann et al., 2014; Lykousis et al., 2009); an in situ observatory monitored the activity of the Athina MV over two years (Sahling et al., 2016; Menapace et al., 2017). Fluid emission sites in the area of Athina MV were documented during MARUM ROV Dive 135 in 2006 (Bohrmann et al., 2008). Nearby our sampling site, methane seepage and seep-dwelling communities dominated by dense colonies of tubeworms were found at the rim of the SW peak of Athina MV (Fig. 2).

Materials and methods

The TCC was sampled at the SW peak of Athina MV (sample GeoB11319-1; 35°23.279’N, 30°12.644’E) at 1794 m water depth (Fig. 1B), using the manipulator arm of the ROV MARUM QUEST during the RV METEOR M70/3 expedition (Bohrmann et al., 2008). Subsamples for the different analytical investigations have been prepared from GeoB11319-1 (Suppl. Mat.). Thin-sections were prepared from cut slabs embedded

in epoxy resin for standard petrographic analyses on a Zeiss Axioskop 40A microscope equipped with a digital camera. Thin sections were partly stained with Feigl's solution in order to highlight textural and mineralogical features.

Sample powders for X-ray diffraction (XRD) and for stable isotope measurements were obtained from surfaces of the polished slabs, using a handheld microdrill (Fig. 1-2S). The XRD measurements were performed on a X'PERT PRO diffractometer equipped with a copper anode $\lambda = 1.54$ Å at 40 mA and 40 kV current. Qualitative and quantitative analyses were carried out applying the Rietveld method using EXPGUI-GSAS (Rietveld, 1969; Larson and von Dreele, 1994; Toby, 2001). The accuracy was estimated ± 1 wt.-%. The Mg-content in calcite was determined using the method of Titschack et al. (2011).

Oxygen and carbon stable isotopes were analysed with a Finnigan MAT 251 mass spectrometer connected to a Kiel I automated carbonate preparation device. Sample powder was reacted with 100% phosphoric acid at 75° C. Accuracy and precision were checked by repeated measurements of an internal standard (ground Solnhofen limestone) calibrated against the NBS19 standard. Long-term standard deviation was estimated to be smaller than 0.05‰ $\delta^{13}C$, and 0.07‰ $\delta^{18}O$. The ratios of $^{18}O/^{16}O$ and $^{13}C/^{12}C$ are reported in the δ-notation in ‰ relative to the Vienna-Pee Dee Belemnite (V-PDB) standard.

Total lipid extracts (TLE) of samples A and B (Fig. 3S) were obtained applying the preparation, decalcification, extraction, and separation procedures published by Birgel et al. (2006; 2008). An aliquot of the TLE was separated into different lipid compound classes (i.e., hydrocarbons, ketones, alcohols, fatty acids) by solid phase extraction based on column chromatography using amino propyl columns. Prior to gas chromatographic analysis, alcohols and fatty acids were derivatized by forming trimethylsilyl (TMS) ethers and methyl esters, respectively. For preparation of biphytanes from glycerol dialkyl glycerol tetraethers (GDGTs), an aliquot of the alcohol fraction was subjected to ether cleavage via HI treatment and reduction of the intermediately formed iodides with $LiAlH_4$ under argon atmosphere. The fractions were examined using a Thermo Electron Trace gas chromatography–mass spectrometer (GC-MS) equipped with a 30 m Restek Rxi-5MS fused silica capillary column (0.25 mm i.d., 0.25 μm film thickness). The carrier gas was helium and the GC temperature program used was as follows: 60 °C, 1 min isothermal; from 60 to 150 °C at 10 °C min^{-1}; from 150 to 320°C at 4° min^{-1}, 22 min isothermal. Compound identification was based on relative GC retention times and mass spectra in comparison with published data. Compound-specific carbon

136 isotopes were measured using a GC-isotope ratio MS (GC-IRMS; Thermo Scientific V Delta Plus with Trace
137 GC ultra-connected via GC Isolink and ConFlo IV interfaces) with GC conditions being identical to those
138 above described. Carbon isotopes are given as δ-values ($\delta^{13}C$) in ‰ relative to the V-PDB standard with a
139 precision of <1‰ based on regular analysis of an *n*-alkane lab standard. $\delta^{13}C$ values of TMS-ethers and fatty
140 acid methyl esters (FAMEs) were corrected for additional carbon atoms introduced during derivatization. An
141 aliquot of the underivatized alcohol fraction was used for high performance liquid chromatography-MS
142 analysis (HPLC-MS) of core GDGT distributions which was conducted using the detailed protocol and
143 equipment described in Becker et al. (2013). The amount of cyclopentane rings in GDGT was monitored by
144 applying the Methane Index (MI) according to Zhang et al. (2011).
145
146 **Results**
147 *Seafloor observations*
148 The seafloor observations of the SW peak of Athina MV showed widespread authigenic carbonate crusts
149 with abundant colonies of the siboglinid tubeworms, previously identified as *Lamellibrachia anaximandri*
150 (Southward et al., 2011), including a high-dense giant colony, the largest so far discovered in the
151 Mediterranean sea (Fig. 2). The sample under study was collected from a cluster of TCC forming a unique
152 arrangement of conduits (ca. 60cm high, 1.5 m wide) (Fig. 3), a few meters from living *L.anaximandri*
153 colonies, enclosed under the border of a carbonate crusts. The sampled TCC is about 18x10x7cm (originally
154 ca. 30 cm long, Bohrmann and and cruise participants, 2008) and is composed of numerous elongated, gently
155 curved empty tubes of cemented sediment (Fig. 3B). Internal diameters vary from 1 to 9 mm. The relatively
156 larger tubes (6 to9 mm in diameter) are interconnected with and branched by relatively smaller tubes (2 to3
157 mm in diameter), forming overall a rigid though highly porous framework. Occasionally, tubes were partially
158 filled by unconsolidated fine sediment
159
160 *Mineralogy and petrography*
161 Carbonates and minor silicates (quartz and clay minerals) are main mineral components of the TCC
162 subsamples (Table 1). Magnesian calcite (Mg mol% > 5%) is the major authigenic carbonate mineral (57–77
163 wt.-%) that cements the outer portion of the tubes. Other minor carbonate phases are represented by Mn-

carbonate kutnahorite (2–25 wt.-%), aragonite (2–17 wt.-%), and calcite (6–10 wt.-%). Calcite mainly forms the detrital infilling (0-A1 subsample) (Table 1).

Combined thin section microscopy and XRD results reveal three distinct microfacies (Fig. 4): (i) microcrystalline Mg calcite (M) forming the exterior of the tube cementing enclosing hemipelagic sediment with abundant foraminifera and silt-sized quartz grains; (ii) clotted and fibrous aragonite (cfA) lining the internal tube wall, and (iii) poorly-lithified late detrital infill (Di) partially filling the cavity of the tubes. (Fig. 4B, C). The cfA-Di boundary is sharp, marked by dark-reddish minerals, while observations in stained thin-section show interfingering of cfA with the micritic microfacies (M) (Fig. 4B, C).

Carbonate $\delta^{13}C$ and $\delta^{18}O$

The $\delta^{13}C$ and $\delta^{18}O$ values of the carbonate phases range between –14.4 and +2.7‰ and +2.4 and +3.4‰, respectively (Fig. 5). The lowest $\delta^{13}C$ values –14.4 and –10.2‰ were obtained from the interior tube coating cfA cement (n=2). Mg-calcite-cemented hemipelagic sediment was slightly less ^{13}C-depleted, with $\delta^{13}C$ values ranging from –12.9 to –5 ‰ (n=12). The $\delta^{13}C$ values of the Di (n=4) are positive in the range from 2.2 to 2.7‰. Overall, all samples exhibit similar positive $\delta^{18}O$ values between 2.5 to 3.5‰.

Lipid biomarker

The two TCC subsamples analysed contain various lipid biomarker compounds related to multiple putative sources including those specific for anaerobic methanotrophs (ANME) and sulfate-reducing bacteria (SRB) (Table 2). Overall, representative compounds exhibit a wide range in $\delta^{13}C$ values from −89.8 to −20.2‰. Most strongly ^{13}C-depleted signals were measured for ANME-derived archaeol and SRB-derived DAGE C_{30} containing two *ai*-15:0 side chains. PMI and ether-cleavage derived Bp-0 and -1 yielded less negative $\delta^{13}C$ values between −49.3 and −40.2‰ and between −61.2 and −54.4‰, respectively. The samples also showed a high quantity and variety of lipid biomarkers derived from marine algae, planktonic archaea, terrestrial plants and other anaerobic bacteria (i.e., phytane and cholesterol, Bp-Cren, C_{27} *n*-alkane and *ai*-$C_{15:0}$ fatty acid, respectively) with $\delta^{13}C$ values, ranging from −32.2 to −20.2‰. The intensities of lipid biomarkers derived from AOM-consortia are minor compared to other sources (Fig. 6).

HPLC-MS analysis of the alcohol fraction revealed the highest abundance for GDGT-0 and 5

HPLC-MS analysis of the alcohol fraction revealed a relatively high abundance of GDGT-0 (caldarchaeol) and 5 (crenarchaeol), a GDGT distribution indicative of planktonic archaea (Fig. 6; e.g. Koga et al., 1993; Sinninghe Damste et al., 2002). However, we also found relatively elevated amounts of GDGT-1 and -2 as indicators of ANME species (e.g. Blumenberg et al., 2004), resulting in MI values between 0.52 and 0.58 and thus highlighting intense methane cycling in our samples (Zhang et al., 2011).

Discussion

Carbonate mineralogy and isotopic composition

Two ^{13}C-depleted carbonate phases form the TCC: micritic Mg-calcite (M) building the external surface of the tubes and cementing enclosing sediment and clotted and fibrous aragonite (cfA) lining the inner tube surface (Fig. 4). ^{13}C-depleted Mg-calcite has been frequently found associated with active cold seeps at various MVs and widely reported for the eastern Mediterranean (Aloisi et al., 2000; Bayon et al., 2007). The micritic microfacies (M) includes planktonic foraminifera, therefore, it can be considered partially microbioclastic, (Fig. 4). The δ^{13}C values of the Mg-calcite (–12.9 to –5.0 ‰) and clotted aragonite (–14.4 and –10.2‰) are markedly lower than the δ^{13}C values of the detrital infilling (Di) (2.2 to 2.7‰), identifying different carbon sources for carbonate precipitation. AOM produces ^{13}C-depleted dissolved inorganic carbon (DIC) in the pore-water, driving the precipitation of authigenic carbonates with δ^{13}C values as low as –25 ‰, whereas carbonates that form mainly from seawater are characterized by higher δ^{13}C values of ≈ 0-1 ‰ (Irwin et al., 1977; Swart, 2008). The δ^{13}C values of Athina MV conduits therefore point to the AOM as a relevant DIC-forming process, although mixed with more ^{13}C-enriched sources (i.e. seawater DIC).

Temperature and oxygen isotope composition of seawater control the oxygen isotope fractionation during aragonite precipitation. Consequently, theoretical temperatures during aragonite precipitation can be determined using the δ^{18}O values of the aragonitic phase, applying the equation of Grossman and Ku (1986). Based on the δ^{18}O value obtained from examined aragonite subsamples and the values of $\delta^{18}O_{SMOW}$ of the regional bottom water (1.6‰; Charlou et al., 2003), the resulting equilibrium temperature is estimated to be ≈12.6 °C. This is in good agreement with present day bottom water temperatures of 13°C in the eastern Mediterranean Sea, and confirms aragonite precipitation at seafloor temperatures (cf. Aloisi et al., 2000).

220 *AOM-induced TCC formation*

221 Our results suggest a relevant role of AOM contributing to TCC formation. The TCC subsamples preserved
222 specific lipid biomarker information of AOM and associated ANME/SRB consortia (Table 2). Of these,
223 archaeol and its most negative $\delta^{13}C$ values of ~−90‰ point to the activity of ANMEs, while less ^{13}C-
224 depleted DAGE C_{30} highlights the involvement of SRBs (e.g. Hinrichs et al., 2000; Pancost et al., 2001;
225 Elvert et al., 2005; Niemann and Elvert, 2008). The presence of strongly ^{13}C-depleted archaeol underlines
226 that AOM was likely inducing carbonate precipitation, thus facilitating early lithification of the TCC. The
227 occurrence of DAGEs has been observed in both ANME-1 (i.e. Aloisi et al., 2002; Stadnitskaia et al., 2005;
228 Bouloubassi et al., 2006). and ANME-2 dominated systems (i.e. Nauhaus et al., 2007; Chevalier et al., 2010,
229 2011), although different DAGEs have been found in the two ANME clusters (Blumenberg et al., 2004;
230 Elvert et al., 2005). This points towards the presence of non-AOM-related DAGE-producing SRB, especially
231 abundant in ANME-1-dominated environments, probably being heterotrophic SRB (Grossi et al., 2015;
232 Vinçon-Laugier et al., 2016), which have been shown to produce DAGEs others than found in ANME-2
233 (Nauhaus et al., 2006) and which may potentially thrive on AOM-produced biomass or organic metabolites
234 thereof. Additionally, some studies elucidating on geomicrobiological processes of AOM tend to highlight
235 the low and potentially null direct involvement of SRB in methane oxidation (Milucka et al., 2012; Scheller
236 et al., 2016).
237 The occurrence of strong ^{13}C-depleted PMI is usually ascribed to ANME (Elvert et al., 2000; Chevalier et al.,
238 2013; Miyajima et al., 2018), although these isoprenoids can show highly variable $\delta^{13}C$ values (Birgel et al.,
239 2008), potentially indicating multiple source organisms. Indeed, PMI has also been identified in
240 methanogenic archaea (Tornabene et al., 1979; Schouten et al., 1997), thus very likely explaining the relative
241 high $\delta^{13}C$ values compared to archaeol found in the TCC from Athina MV (Tab. 2).
242 GDGTs containing ^{13}C-depleted biphytane moieties have been frequently reported as major biomarker
243 components at methane seeps (Pancost et al., 2001; Blumenberg et al., 2004; Niemann and Elvert, 2008).
244 GDGTs have been shown to indicate a high impact of methane cycling when the relative amount of
245 characteristic GDGTs expressed via the MI is higher than 0.3 (Zhang et al., 2011), as observed in the TCC
246 samples from Athina MV. More specifically, the lack of crocetane and the occurrence of a GDGT
247 distribution with a high abundance of GDGT-1 and -2 as found in both samples highlights the presence of

archaea of the ANME-1 cluster (Blumenberg et al., 2004; Birgel et al., 2008; Niemann and Elvert, 2008; Rossel et al., 2008). ANME-1 archaea are known to be able to cope with lower methane concentrations than ANME-2 archaea (Blumenberg et al., 2004; Nauhaus et al., 2005; Stadnitskaia et al., 2005; Rossel et al., 2011), which likely gives them advantage at seeps with a diffusive methane flow. The occurrence of an ANME-1 specific GDGT distribution together with a moderate MI value in comparison to many other methane-impacted environments (Zhang et al., 2011) thus suggests that a continuously low methane flux occurred during the formation of the TCC. The intensity of the sub-seafloor hydrocarbon rich fluids may be also related to the mineralogy of the seep carbonates: diffusive methane flow is most likely associated with high-Mg calcite, and effusive turnover is accompanied with aragonite-predominant seep carbonates (i.e. Peckmann et al., 2009; Haas et al., 2010; Guan et al., 2013; Miyajima et al., 2018). However, in our study lipid biomarker analyses have been carried out on bulk subsamples, thus making it difficult to discern strict relationships between mineralogy and potential fluid flow. Nonetheless, the lipid biomarker results coupled with petrographic and mineral observations, allow some further considerations. The much higher amount of lipid biomarkers derived from sources other than AOM (i.e. algae, planktonic archaea, terrestrial input, Fig. 6) suits well with the high amount of the Mg-calcite-rich micritic phase composing the external portion of the tubes. This indicates that a considerable portion of this carbonate phase is unrelated to AOM. Consequently, the AOM-related biomarkers are likely concentrated in the authigenic aragonitic cfA microfacies occurring in the inner tube walls and interfingering with the micrite (Fig. 4). Indeed, the aragonite-rich microfacies is slightly more ^{13}C-depleted compared to Mg-calcite (Fig. 4), but less ^{13}C-depleted than methane-derived aragonite reported in seep-deposits associated with eastern Mediterranean MVs (Aloisi et al., 2000; Peckmann and Thiel, 2004; Himmler et al., 2011). These observations support the hypothesis that the aragonite-rich phase formed the TCC within a context where methane-rich fluids mixed with seawater. Therefore, TCC at Athina MV may represent the termination of the fluid plumbing system below the carbonate crusts where they had been sampled (Fig. 2A).

On the origin of TCC

In order to better constrain processes leading to the formation of the studied TCC, a revision of the TCC described in literature is necessary. Considering the definition of TCC as tubular conduits formed by

the precipitation of authigenic seep-carbonates derived from upward-migrating hydrocarbon-rich fluids, and comparing information from seep-associated carbonates in modern and ancient deposits (see compilation Appendix I, Suppl. Mat.), different formation processes can be outlined. TCCs show a wide variability in terms of size, morphology and settings, ascribing to the following types (Fig. 6,): (i) tubeworms fossils; (ii) ichnological traces of burrowing organisms; (iii) seafloor chimneys (standing up structures formed above the seafloor), (v) pseudo-chimneys ("chimney-like" structures formed in the sediment column and late exposed by the prevailing bottom regime, in the modern marine settings, or exposed on the field in the fossil sites, due to preferential erosion of the surrounding sediments); (vi) sub-seafloor tubular concretions formed as fluid migration pathways (mostly observed in the fossil record).

TCCs described as pseudo-chimneys or sub-seafloor tubular concretions show sizes and morphology (i.e. De Boever et al., 2006; Nyman et al., 2010; Angeletti et al., 2015) referable to deeper portions of a seepage system, excluding this as potential explanation for the formation of the TCC from Athina MV. Chimneys *in sensu stricto* have an internal structure and specific conditions of formation (i.e. anoxic conditions at the seafloor, Peckmann et al., 2001; Bayon et al., 2013) inconsistent with the formation process of TCCs in our samples. At Athina MV, most likely the two following processes may account for the formation of the TCC: mineralization of seep-related tubeworm and lithification of burrows (Fig. 7).

The TCC observed at Athina MV have been previously interpreted as fossil tubeworms based on different reasons (Brinkmann, 2007; Bohrmann et al., 2008). ROV observations documented several bush-like colonies of *L. anaximandri* tubeworms near the sampling site (Fig. 2). Having no digestive system, the tubeworms are sustained by exchanging chemical compounds with the surrounding environment (McMullin et al., 2003; Cordes et al., 2005; Bright and Lallier, 2010). In particular, the "roots", the sediment-buried portion of the tubeworms, are responsible for the uptake of dissolved hydrogen sulphide from the surrounding pore water (Julian et al., 1999; Freytag et al., 2001) while oxygen and carbon dioxide are taken up from bottom seawater through the brachial plume (Dattagupta et al., 2008). The diameters, the tapering morphology and the cluster aspect of the TCC are comparable with the buried portion of the roots of the *L.anaximandri* colonies, as observed in other Mediterranean seepage sites (Nile Delta, Römer et al., 2014; Calabrian Arc, Bohrmann et al., 2015). However, the TCC is a framework composed of interconnected and dendritic-shaped conduits (branching secondary tubes, Fig. 3) and the conduits do not contain any chitinous

304 remains, making them unlikely to be remnants of the past occurrence of tubeworm individuals (Haas et al.,
305 2009; Southward et al., 2011). Additionally, the tubeworm physiology requires favourable geochemical
306 conditions characterized by relatively high production of hydrogen sulphide, guaranteed by high AOM-rates.
307 The latter is not consistent with our data, considering the more ^{13}C-enriched composition of carbonates,
308 specifically cfA, and the low abundance of specific lipid biomarkers of AOM consortia.
309 In contrast, the TCC from Athina MV share similarities in terms of size and shape with lithified burrows,
310 acting as fluid conduits in the pockmarks of the Mediterranean Sea and Congo deep-sea fan (Haas et al.,
311 2010; Taviani et al., 2013). Likewise, in ancient seep deposits, TCCs have been described as methane-
312 derived authigenic carbonate cementations of burrows related to fluid seepage (Wiese et al., 2015; Zwicker
313 et al., 2015). The lack of different aragonitic laminations filling the conduit, as observed by Zwicker et al.
314 (2015) could suggests a low discharge of hydrocarbon-rich fluids from the SW peak of Athina, agreeing with
315 our results obtained from the carbonate stable isotopes and lipid biomarkers. The hypothesis of the origin of
316 TCC as mineralization of buried portion of tubeworms seems unlikely following the results discussed in this
317 work. The ichnological activity of burrowing organisms (i.e. seep-dwelling decapod, Taviani et al., 2013)
318 represents the most reasonable process for the formation of the peculiar framework of interconnected and
319 branching TCC from Athina MV. Our findings, discussed with observations made at modern seep
320 environments, highlights how hydrocarbon seepage in the shallow subsurface can exploit structures related
321 to macrofaunal activity as conduits.
322

323 **Conclusion**

324 Tubular carbonate conduits (TCCs) sampled from the Athina MV in the eastern Mediterranean Sea likely
325 represent early-lithified burrows. ^{13}C-depleted Mg-calcite and aragonite are the dominant carbonate phases
326 comprising the TCC framework. Stable carbon and oxygen isotope composition of the carbonate phases
327 indicate that sulfate-reduction processes induced authigenic carbonate precipitation at bottom water
328 temperatures. Specific ^{13}C-depleted lipid biomarkers of ANME-1/SRB consortia suggest that sulfate-
329 dependent AOM facilitated carbonate precipitation and the preservation of the conduits. However, AOM
330 activity was limited due to the minor abundance of AOM-related biomarkers relatively to background
331 organic matter input. We show how fluid leakage from the sub-seafloor at seepage environments can be

highly influenced by the activity of burrowing organisms. Our observations confirm that TCC likely formed by the action of burrowing organism rather than being mineralizations of tubeworm colonies, albeit these are widely observed at Athina MV. These findings offer a comprehensive review for better understanding of TCC origin and role within a modern and past hydrocarbon seep settings.

Acknowledgements

Skilful work of the captain and crew members, as well as the MARUM-QUEST 4000 team during RV METEOR cruise M70⁄3 and the MARUM AUV team during R/V POSEIDON cruise P462 are greatly appreciated. Thanks go to Monika Segl (University of Bremen) for analytical support. Prof. Dierk Hebbeln (MARUM) is acknowledged for his general support. Funding for T.H., M.E., and G.B. was provided through the DFG-Research Center⁄Cluster of Excellence 'The Ocean in the Earth Systems'. E.U. programme "LLP-Erasmus Placement 2013" (University of Modena and Reggio Emilia, Italy) provided funding for L.T. We thank the journal editor V. Blinova for handling our work. The quality of this manuscript has been significantly improved by the comments and suggestions of D. Oppo and two anonymous reviewers.

References

Aksu, A.E., Hall, J., and Yaltirak, C., 2009, Miocene-Recent evolution of Anaximander Mountains and Finike Basin at the junction of Hellenic and Cyprus Arcs, eastern Mediterranean: Marine Geology, v. 258, p. 24–47, doi: 10.1016/j.margeo.2008.04.008.

Aloisi, G., Bouloubassi, I., Heijs, S.K., Pancost, R.D., Pierre, C., Sinninghe Damsté, J.S., Gottschal, J.C., Forney, L.J., and Rouchy, J.M., 2002, CH_4-consuming microorganisms and the formation of carbonate crusts at cold seeps: Earth and Planetary Science Letters, v. 203, p. 195–203, doi: 10.1016/S0012-821X(02)00878-6.

Aloisi, G., Pierre, C., Rouchy, J.M., Foucher, J.P., and Woodside, J., 2000, Methane-related authigenic carbonates of Eastern Mediterranean Sea mud volcanoes and their possible relation to gas hydrate destabilisation: Earth and Planetary Science Letters, v. 184, p. 321–338, doi: 10.1016/S0012-

821X(00)00322-8.

Angeletti, L., Canese, S., Franchi, F., Montagna, P., Reitner, J., and Walliser, E.O., 2015, The “chimney forest ” of the deep Montenegrin margin, south-eastern Adriatic Sea: Marine and Petroleum Geology, v. 66, p. 542–554, doi: 10.1016/j.marpetgeo.2015.04.001.

Argentino, C., Conti, S., Crutchley, G.J., Fioroni, C., Fontana, D., and Johnson, J.E., 2019, Methane-derived authigenic carbonates on accretionary ridges: Miocene case studies in the northern Apennines (Italy) compared with modern submarine counterparts: Marine and Petroleum Geology, v. 102, p. 860–872, doi: 10.1016/J.MARPETGEO.2019.01.026.

Bahr, A., Pape, T., Bohrmann, G., Mazzini, A., Haeckel, M., Reitz, A., and Ivanov, M., 2009, Authigenic carbonate precipitates from the NE Black Sea: a mineralogical, geochemical, and lipid biomarker study: International Journal of Earth Sciences, v. 98, p. 677–695, doi: 10.1007/s00531-007-0264-1.

Bayon, G., Dupré, S., Ponzevera, E., Etoubleau, J., Chéron, S., Pierre, C., Mascle, J., Boetius, A., and de Lange, G.J., 2013, Formation of carbonate chimneys in the Mediterranean Sea linked to deep-water oxygen depletion: Nature Geoscience, v. 6, p. 755–760, doi: 10.1038/ngeo1888.

Bayon, G., Pierre, C., Etoubleau, J., Voisset, M., Cauquil, E., Marsset, T., Sultan, N., Le Drezen, E., and Fouquet, Y., 2007, Sr/Ca and Mg/Ca ratios in Niger Delta sediments: Implications for authigenic carbonate genesis in cold seep environments: Marine Geology, v. 241, p. 93–109, doi: 10.1016/j.margeo.2007.03.007.

Becker, K.W., Lipp, J.S., Zhu, C., Liu, X.L., and Hinrichs, K.U., 2013, An improved method for the analysis of archaeal and bacterial ether core lipids: Organic Geochemistry, v. 61, p. 34–44, doi: 10.1016/j.orggeochem.2013.05.007.

Birgel, D., Elvert, M., Han, X., and Peckmann, J., 2008, ^{13}C-depleted biphytanic diacids as tracers of past anaerobic oxidation of methane: Organic Geochemistry, v. 39, p. 152–156, doi: 10.1016/j.orggeochem.2007.08.013.

Birgel, D., Thiel, V., Hinrichs, K.U., Elvert, M., Campbell, K.A., Reitner, J., Farmer, J.D., and Peckmann, J.,

2006, Lipid biomarker patterns of methane-seep microbialites from the Mesozoic convergent margin of California: Organic Geochemistry, v. 37, p. 1289–1302, doi: 10.1016/j.orggeochem.2006.02.004.

Blumenberg, M., Seifert, R., Reitner, J., Pape, T., and Michaelis, W., 2004, Membrane lipid patterns typify distinct anaerobic methanotrophic consortia: Proceedings of the National Academy of Sciences, v. 101, p. 11111–11116, doi: 10.1073/pnas.0401188101.

Boetius, A., Ravenschlag, K., Schubert, C.J., Rickert, D., Widdel, F., Gieseke, A., Amann, R., Jørgensen, B.B., Witte, U., and Pfannkuche, O., 2000, A marine microbial consortium apparently mediating anaerobic oxidation of methane.: Nature, v. 407, p. 623–626, doi: 10.1038/35036572.

De Boever, E., Huysmans, M., Muchez, P., Dimitrov, L., and Swennen, R., 2009, Controlling factors on the morphology and spatial distribution of methane-related tubular concretions – Case study of an Early Eocene seep system: Marine and Petroleum Geology, v. 26, p. 1580–1591, doi: 10.1016/j.marpetgeo.2008.11.004.

De Boever, E., Swennen, R., and Dimitrov, L., 2006, Lower Eocene carbonate cemented chimneys (Varna, NE Bulgaria): Formation mechanisms and the (a)biological mediation of chimney growth? Sedimentary Geology, v. 185, p. 159–173, doi: 10.1016/j.sedgeo.2005.12.010.

Bohrmann, G., Abegg, F., Bahr, A., Bergenthal, M., Brüning, M., Brinkmann, F., Dentrecolas, S., A., F., Gassner, A., Hessler, S., Hohnberg, H.J., Hüttich, D., Illhan, T., Klapp, S.A., et al., 2008, Report and preliminary results of R/V METEOR Cruise M70/3, Iraklion – Iraklion, 21 November – 8 December, 2006. Cold seeps of the Anaximander Mountains / Eastern Mediterranean. Berichte, Fachbereich Geowissenschaften, Universität Bremen, No. 262, 75 pages: Berichte Fachbereich Geowissenschaften Universität Bremen, p. 75.

Bohrmann, G., Alijuhne, K., Dehning, K., Ferreira, C., Feseker, T., Gürcan, E.S., Hacioğlu, E., Leymann, G., Meinecke, G., Pape, T., Renken, J., Römer, M., Spiesecke, U., and von Wahl, T., 2014, Report and Preliminary Results of R/V POSEIDON Cruise P462, Izmir – Izmir, 28 October – 21 November, 2013. Gas hydrate dynamics of mud volcanoes in the submarine Anaximander Mountains (Eastern Mediterranean).:

Bohrmann, G., Alvarez, R., Biller, T., Buchheister, S., Büttner, H., Canoni, O., Dehning, K., Ferreira, C., Geprägs, P., Heinken, S., Hüttich, D., Johansen, C., Klar, S., Klüber, S., et al., 2015, Report and preliminary results of R/V METEOR cruise M112, Dynamic of mud volcanoes and seeps in the Calabrian accretionary prism, Ionian Sea, Catania (Italy) – Catania (Italy), November 6 – December 15, 2014.: Berichte, MARUM – Zentrum für Marine Umweltwissenschaften, Fachbereich Geowissenschaften, Universität Bremen, No. 306, 217 pages. Bremen, 2015. ISSN 2195-9633., p. 217.

Bohrmann, G., and Greinert, J., 1998, Authigenic carbonates from the Cascadia subduction zone and their relation to gas hydrate stability: v. 18, p. 647–650.

Bouloubassi, I., Aloisi, G., Pancost, R.D., Hopmans, E., Pierre, C., and Sinninghe Damsté, J.S., 2006, Archaeal and bacterial lipids in authigenic carbonate crusts from eastern Mediterranean mud volcanoes: Organic Geochemistry, v. 37, p. 484–500, doi: 10.1016/j.orggeochem.2005.11.005.

Bright, M., and Lallier, F.H., 2010, The biology of vestimentiferan tubeworms: Oceanography and Marine Biology, v. 48, p. 213–266, doi: 10.1201/EBK1439821169-c4.

Brinkmann, F., 2007, Genesis of carbonate crusts at cold seeps of eastern Mediterranean Sea mud volcanoes: Master Thesis, University of Bremen, Germany, Bremen,.

Campbell, K.A., 2006, Hydrocarbon seep and hydrothermal vent paleoenvironments and paleontology: Past developments and future research directions: Palaeogeography, Palaeoclimatology, Palaeoecology, v. 232, p. 362–407, doi: 10.1016/j.palaeo.2005.06.018.

Charlou, J.L., Donval, J.P., Zitter, T., Roy, N., Jean-Baptiste, P., Foucher, J.P., and Woodside, J., 2003, Evidence of methane venting and geochemistry of brines on mud volcanoes of the eastern Mediterranean Sea: Deep-Sea Research Part I: Oceanographic Research Papers, v. 50, p. 941–958, doi: 10.1016/S0967-0637(03)00093-1.

Chevalier, N., Bouloubassi, I., Birgel, D., Crémière, A., Taphanel, M.H., and Pierre, C., 2011, Authigenic carbonates at cold seeps in the Marmara Sea (Turkey): A lipid biomarker and stable carbon and oxygen isotope investigation: Marine Geology, v. 288, p. 112–121, doi: 10.1016/j.margeo.2011.08.005.

435 Chevalier, N., Bouloubassi, I., Birgel, D., Taphanel, M.H., and López-García, P., 2013, Microbial methane
436 turnover at Marmara Sea cold seeps: A combined 16S rRNA and lipid biomarker investigation:
437 Geobiology, v. 11, p. 55–71, doi: 10.1111/gbi.12014.

438 Chevalier, N., Bouloubassi, I., Stadnitskaia, A., Taphanel, M.H., Lorre, A., Damsté, J.S., and Pierre, C.,
439 2010, Distributions and carbon isotopic compositions of lipid biomarkers in authigenic carbonate crusts
440 from the Nordic margin (Norwegian Sea): Organic Geochemistry, v. 41, p. 885–890, doi:
441 10.1016/j.orggeochem.2010.03.012.

442 Conti, S., Fontana, D., Lucente, C.C., and Pini, G.A., 2014, Relationships between seep-carbonates, mud
443 volcanism and basin geometry in the Late Miocene of the northern Apennines of Italy: The Montardone
444 mélange: International Journal of Earth Sciences, v. 103, p. 281–295, doi: 10.1007/s00531-013-0928-y.

445 Cordes, E.E., Arthur, M.A., Shea, K., Arvidson, R.S., and Fisher, C.R., 2005, Modeling the mutualistic
446 interactions between tubeworms and microbial consortia: PLoS Biology, v. 3, p. 0497–0506, doi:
447 10.1371/journal.pbio.0030077.

448 Dattagupta, S., Arthur, M.A., and Fisher, C.R., 2008, Modification of sediment geochemistry by the
449 hydrocarbon seep tubeworm *Lamellibrachia luymesi*: A combined empirical and modeling approach:
450 Geochimica et Cosmochimica Acta, v. 72, p. 2298–2315, doi: 10.1016/j.gca.2008.02.016.

451 Dimitrov, L., 2002, Mud volcanoes – the most important pathways for degassing deeply buried sediments:
452 Earth Science Review, v. 59, p. 49–76, doi: 10.1016/S0012-8252(02)00069-7.

453 Elvert, M., Hopmans, E.C., Treude, T., Boetius, A., and Suess, E., 2005, Spatial variations of
454 methanotrophic consortia at cold methane seeps: Implications from a high-resolution molecular and
455 isotopic approach: Geobiology, v. 3, p. 195–209, doi: 10.1111/j.1472-4669.2005.00051.x.

456 Elvert, M., Suess, E., Greinert, J., and Whiticar, M.J., 2000, Archaea mediating anaerobic methane oxidation
457 in deep-sea sediments at cold seeps of the eastern Aleutian subduction zone: Organic Geochemistry, v.
458 31, p. 1175–1187, doi: 10.1016/S0146-6380(00)00111-X.

459 Elvert, M., Suess, E., and Whiticar, M.J., 1999, Anaerobic methane oxidation associated with marine gas

460 hydrates: superlight C-isotopes from saturated and unsaturated C_{20} and C_{25} irregular isoprenoids:
461 Naturwissenschaften, v. 86, p. 295–300, doi: 10.1007/s001140050619.

462 Freytag, J.K., Girguis, P.R., Bergquist, D.C., Andras, J.P., Childress, J.J., and Fisher, C.R., 2001, A paradox
463 resolved: sulfide acquisition by roots of seep tubeworms sustains net chemoautotrophy: Proceedings of
464 the National Academy of Sciences of the United States of America, v. 98, p. 13408–13, doi:
465 10.1073/pnas.231589498.

466 Grossi, V., Mollex, D., Vinçon-Laugier, A., Hakil, F., Pacton, M., and Cravo-Laureau, C., 2015, Mono- and
467 dialkyl glycerol ether lipids in anaerobic bacteria: Biosynthetic insights from the mesophilic sulfate
468 reducer Desulfatibacillum alkenivorans PF2803^T: Applied and Environmental Microbiology, v. 81, p.
469 3157–3168, doi: 10.1128/AEM.03794-14.

470 Grossman, E.L., and Ku, T.-L., 1986, Oxygen and carbon isotope fractionation in biogenic aragonite:
471 temperature effects: Chemical Geology (Isotope Geoscience Section), v. 59, p. 59–74, doi:
472 10.1016/0168-9622(86)90057-6.

473 Guan, H., Sun, Y., Zhu, X., Mao, S., Feng, D., Wu, N., and Chen, D., 2013, Factors controlling the types of
474 microbial consortia in cold-seep environments: A molecular and isotopic investigation of authigenic
475 carbonates from the south china sea: Chemical Geology, v. 354, p. 55–64, doi:
476 10.1016/j.chemgeo.2013.06.016.

477 Haas, A., Little, C.T.S., Sahling, H., Bohrmann, G., Himmler, T., and Peckmann, J., 2009, Mineralization of
478 vestimentiferan tubes at methane seeps on the Congo deep-sea fan: Deep-Sea Research Part I:
479 Oceanographic Research Papers, v. 56, p. 283–293, doi: 10.1016/j.dsr.2008.08.007.

480 Haas, A., Peckmann, J., Elvert, M., Sahling, H., and Bohrmann, G., 2010, Patterns of carbonate authigenesis
481 at the Kouilou pockmarks on the Congo deep-sea fan: Marine Geology, v. 268, p. 129–136, doi:
482 10.1016/j.margeo.2009.10.027.

483 Himmler, T., Birgel, D., Bayon, G., Pape, T., Ge, L., Bohrmann, G., and Peckmann, J., 2015, Formation of
484 seep carbonates along the Makran convergent margin, northern Arabian Sea and a molecular and

485 isotopic approach to constrain the carbon isotopic composition of parent methane: Chemical Geology,
486 v. 415, p. 102–117, doi: 10.1016/j.chemgeo.2015.09.016.

487 Himmler, T., Brinkmann, F., Bohrmann, G., and Peckmann, J., 2011, Corrosion patterns of seep-carbonates
488 from the eastern Mediterranean Sea: Terra Nova, v. 23, p. 206–212, doi: 10.1111/j.1365-
489 3121.2011.01000.x.

490 Himmler, T., Smrzka, D., Zwicker, J., Kasten, S., Shapiro, R.S., Bohrmann, G., and Peckmann, J., 2018,
491 Stromatolites below the photic zone in the northern Arabian Sea formed by calcifying chemotrophic
492 microbial mats: Geology, v. 46, p. 339–342, doi: 10.1130/G39890.1.

493 Hinrichs, K.U., Summons, R.E., Orphan, V., Sylva, S.P., and Hayes, J.M., 2000, Molecular and isotopic
494 analysis of anaerobic methaneoxidizing communities in marine sediments: Organic Geochemistry, v.
495 31, p. 1685–1701, doi: 10.1016/S0146-6380(00)00106-6.

496 Hoehler, T.M., Alperin, M.J., Albert, D.B., and Martens, C.S., 1994, Field and laboratory studies of methane
497 oxidation in an anoxic marine sediment: Evidence for a methanogen-sulfate reducer consortium: Global
498 Biogeochemical Cycles, v. 8, p. 451–463, doi: 10.1029/94GB01800.

499 Irwin, H., Curtis, C., and Coleman, M., 1977, Isotopic evidence for source of diagenetic carbonates formed
500 during burial of organic-rich sediments: Nature, v. 269, p. 209–213, doi: 10.1038/269209a0.

501 Julian, D., Gaill, F., Wood, E., Arp, a J., and Fisher, C.R., 1999, Roots as a site of hydrogen sulfide uptake
502 in the hydrocarbon seep vestimentiferan *Lamellibrachia* sp.: The Journal of experimental biology, v.
503 202, p. 2245–2257.

504 Koga, Y., Nishihara, M., Morii, H., and Akagawa-Matsushita, M., 1993, Ether polar lipids of methanogenic
505 bacteria: structures, comparative aspects, and biosyntheses.: Microbiological reviews, v. 57, p. 164–
506 182.

507 Kopf, A.J., 2002, Significance of mud volcanism: Reviews of Geophysics, v. 40, p. 1–52, doi:
508 10.1029/2000RG000093.

509 Larson, A.C., and von Dreele, R.B., 1994, General Structure Analysis System (GSAS): Los Alamos National

510 Laboratory Report LAUR 86-748., v. 748.

511 Levin, L.A., 2005, Ecology of cold seep sediments: Interactions of fauna with flow, chemistry and microbes:
512 An Annual Review, v. 43, p. 1–46, doi: doi:10.1201/9781420037449.ch1.

513 Lykousis, V., Alexandri, S., Woodside, J., de Lange, G., Dählmann, A., Perissoratis, C., Heeschen, K.,
514 Ioakim, C., Sakellariou, D., Nomikou, P., Rousakis, G., Casas, D., Ballas, D., and Ercilla, G., 2009,
515 Mud volcanoes and gas hydrates in the Anaximander mountains (Eastern Mediterranean Sea): Marine
516 and Petroleum Geology, v. 26, p. 854–872, doi: 10.1016/j.marpetgeo.2008.05.002.

517 McMullin, E.R., Hourdez, S., Schaeffer, S.W., and Fisher, C.R., 2003, Phylogeny and biogeography of deep
518 sea vestimentiferan tubworms and their bacterial symbionts.: Symbiosis, v. 34, p. 1–41.

519 Menapace, W., Völker, D., Kopf, A., Sahling, H., Zoellner, C., dos Santos Ferreira, C., and Bohrmann, G.,
520 2017, Long-term in situ observations at the Athina mud volcano (Eastern Mediterranean) - taking the
521 pulse of mud volcanism: Tectonophysics, v. 721, p. 12–27, doi: 10.1016/j.tecto.2017.09.010.

522 Michaelis, W., Seifert, R., Nauhaus, K., Treude, T., Thiel, V., Blumenberg, M., Knittel, K., Gieseke, A.,
523 Peterknecht, K., Pape, T., Boetius, A., Amann, R., Jorgensen, B.B., Widdel, F., et al., 2002, Microbial
524 reefs in the Black Sea fueled by anaerobic oxidation of methane: Science, v. 297, p. 1013–1015, doi:
525 10.1126/science.1072502.

526 Milkov, A. V., Sassen, R., Apanasovich, T. V., and Dadashev, F.G., 2003, Global gas flux from mud
527 volcanoes: A significant source of fossil methane in the atmosphere and the ocean: Geophysical
528 Research Letters, v. 30, p. 17–20, doi: 10.1029/2002GL016358.

529 Milucka, J., Ferdelman, T.G., Polerecky, L., Franzke, D., Wegener, G., Schmid, M., Lieberwirth, I., Wagner,
530 M., Widdel, F., and Kuypers, M.M.M., 2012, Zero-valent sulphur is a key intermediate in marine
531 methane oxidation: Nature, v. 491, p. 541–546, doi: 10.1038/nature11656.

532 Miyajima, Y., Ijiri, A., Miyake, A., and Hasegawa, T., 2018, Origin of methane and heavier hydrocarbons
533 entrapped within Miocene methane-seep carbonates from central Japan: Chemical Geology, v. 498, p.
534 83–95, doi: 10.1016/j.chemgeo.2018.09.014.

535 Nauhaus, K., Elvert, M., Widdel, F., Albrecht, M., and Boetius, A., 2006, *In vitro* cell growth of marine
536 archaeal-bacterial consortia during anaerobic oxidation of methane with sulfate: Environmental
537 Microbiology, v. 9, p. 187–196, doi: 10.1111/j.1462-2920.2006.01127.x.

538 Nauhaus, K., Treude, T., Boetius, A., and Krüger, M., 2005, Environmental regulation of the anaerobic
539 oxidation of methane: A comparison of ANME-I and ANME-II communities: Environmental
540 Microbiology, v. 7, p. 98–106, doi: 10.1111/j.1462-2920.2004.00669.x.

541 Niemann, H., and Elvert, M., 2008, Diagnostic lipid biomarker and stable carbon isotope signatures of
542 microbial communities mediating the anaerobic oxidation of methane with sulphate: Organic
543 Geochemistry, v. 39, p. 1668–1677, doi: 10.1016/j.orggeochem.2007.11.003.

544 Nyman, S.L., Nelson, C.S., and Campbell, K.A., 2010, Miocene tubular concretions in East Coast Basin,
545 New Zealand: Analogue for the subsurface plumbing of cold seeps: Marine Geology, v. 272, p. 319–
546 336, doi: 10.1016/j.margeo.2009.03.021.

547 Olu-Le Roy, K., Sibuet, M., Fiala-Médioni, A., Gofas, S., Salas, C., Mariotti, A., Foucher, J.P., and
548 Woodside, J., 2004, Cold seep communities in the deep eastern Mediterranean Sea: Composition,
549 symbiosis and spatial distribution on mud volcanoes: Deep-Sea Research Part I: Oceanographic
550 Research Papers, v. 51, p. 1915–1936, doi: 10.1016/j.dsr.2004.07.004.

551 Orphan, V.J., House, C.H., Hinrichs, K.-U., Mckeegan, K.D., and Delong, E.F., 2001, Methane-consuming
552 archaea revealed by directly coupled isotopic and phylogenetic analysis: Source: Science, New Series
553 Cell Mol. Cell Proc. Natl. Acad. Sci. U.S.A. Nature Cell X. Z. Su et al. Cell D. I. Baruch et al. Cell, v.
554 293, p. 484–487, doi: 10.1126/science.1061338.

555 Pancost, R.D., Damsté, J., Sinninghe, S., Lint, S. De, Maarel, M.J.E.C. Van Der, and Gottschal, J.C., 2000,
556 Biomarker evidence for widespread anaerobic methane oxidation in Mediterranean sediments by a
557 consortium of methaogenic archaea and bacteria: Applied and environmental microbiology, v. 66, p.
558 1126–1132, doi: 10.1128/AEM.66.3.1126-1132.2000.Updated.

559 Pancost, R.D., Hopmans, E.C., Sinninghe Damsté, J.S., and The MEDINAUT Shipboard Scientific Party,

2001, Archaeal lipids in mediterranean cold seeps: Molecular proxies for anaerobic methane oxidation: Geochimica et Cosmochimica Acta, v. 65, p. 1611–1627, doi: 10.1016/S0016-7037(00)00562-7.

Pape, T., Kasten, S., Zabel, M., Bahr, A., Abegg, F., Hohnberg, H.J., and Bohrmann, G., 2010, Gas hydrates in shallow deposits of the Amsterdam mud volcano, Anaximander Mountains, northeastern Mediterranean Sea: Geo-Marine Letters, v. 30, p. 187–206, doi: 10.1007/s00367-010-0197-8.

Peckmann, J., Birgel, D., and Kiel, S., 2009, Molecular fossils reveal fluid composition and flow intensity at a Cretaceous seep: Geology, v. 37, p. 847–850, doi: 10.1130/G25658A.1.

Peckmann, J., Reimer, A., Luth, U., Luth, C., Hansen, B.T., Heinicke, C., Hoefs, J., and Reitner, J., 2001, Methane-derived carbonates and authigenic pyrite from the northwestern Black Sea: Marine Geology, v. 177, p. 129–150, doi: 10.1016/S0025-3227(01)00128-1.

Peckmann, J., and Thiel, V., 2004, Carbon cycling at ancient methane-seeps: Chemical Geology, v. 205, p. 443–467, doi: 10.1016/j.chemgeo.2003.12.025.

Rietveld, H.M., 1969, A profile refinement method for nuclear and magnetic structures: Journal of Applied Crystallography, v. 2, p. 65–71, doi: 10.1107/S0021889869006558.

Römer, M., Sahling, H., Pape, T., dos Santos Ferreira, C., Wenzhöfer, F., Boetius, A., and Bohrmann, G., 2014, Methane fluxes and carbonate deposits at a cold seep area of the Central Nile Deep Sea Fan, Eastern Mediterranean Sea: Marine Geology, v. 347, p. 27–42, doi: 10.1016/j.margeo.2013.10.011.

Rossel, P.E., Elvert, M., Ramette, A., Boetius, A., and Hinrichs, K.U., 2011, Factors controlling the distribution of anaerobic methanotrophic communities in marine environments: Evidence from intact polar membrane lipids: Geochimica et Cosmochimica Acta, v. 75, p. 164–184, doi: 10.1016/j.gca.2010.09.031.

Rossel, P.E., Lipp, J.S., Fredricks, H.F., Arnds, J., Boetius, A., Elvert, M., and Hinrichs, K.U., 2008, Intact polar lipids of anaerobic methanotrophic archaea and associated bacteria: Organic Geochemistry, v. 39, p. 992–999, doi: 10.1016/j.orggeochem.2008.02.021.

Sahling, H., Loher, M., Menapace, W., Voelker, D., Bihler, V., Nowald, N., Seiter, C., Leymann, T., Vittori,

585 V., Darilmaz, E., and Karaaslan, N., 2016, R/V Poseidon Cruise Report POS498 Recovery of
586 observatories at Athina mud volcano.:

587 Sahling, H., Rickert, D., Lee, R.W., Linke, P., and Suess, E., 2002, Macrofaunal community structure and
588 sulfide flux at gas hydrate deposits from the Cascadia convergent margin, NE Pacific: Marine Ecology
589 Progress Series, v. 231, p. 121–138, doi: 10.3354/meps231121.

590 Scheller, S., Yu, H., Chadwick, G.L., McGlym, S.E., and Orphan, V.J., 2016, Artificial electron acceptors
591 decouple archaeal methane oxidation from sulfate reduction: Science, v. 351, p. 703–707, doi:
592 10.1126/science.aad7154.

593 Schouten, S., van der Maarel, M.J.E.C., Huber, R., and Sinninghe Damsté, J.S., 1997, 2,6,10,15,19-
594 Pentamethylicosenes in *Methanolobus bombayensis*, a marine methanogenic arachaeon, and in
595 *Methanosarcina mazei*: Organic Geochemistry, v. 26, p. 409–414.

596 Sibuet, M., and Olu, K., 1998, Biogeography, biodiversity and fluid dependence of deep-sea cold-seep
597 communities at active and passive margins: Deep-Sea Research Part II: Topical Studies in
598 Oceanography, v. 45, p. 517–567, doi: 10.1016/S0967-0645(97)00074-X.

599 Sinninghe Damsté, J.S., Schouten, S., Hopmans, E.C., van Duin, A.C.T., and Geenevasen, J.A., 2002,
600 Crenarchaeol: the characteristic core glycerol dibiphytanyl glycerol tetraether membrane lipid of
601 cosmopolitan pelagic crenarchaeota: The Journal of Lipid Research, v. 43, p. 1641–1651, doi:
602 10.1194/jlr.M200148-JLR200.

603 Southward, E.C., Andersen, A.C., and Hourdez, S., 2011, *Lamellibrachia anaximandri* n. Sp., a new
604 vestimentiferan tubeworm (Annelida) from the Mediterranean, with notes on frenulate tubeworms from
605 the same habitat: Zoosystema, v. 33, p. 245–279, doi: 10.5252/z2011n3a1.

606 Stadnitskaia, A., Muyzer, G., Abbas, B., Coolen, M.J.L., Hopmans, E.C., Baas, M., Van Weering, T.C.E.,
607 Ivanov, M.K., Poludetkina, E., and Sinninghe Damsté, J.S., 2005, Biomarker and 16S rDNA evidence
608 for anaerobic oxidation of methane and related carbonate precipitation in deep-sea mud volcanoes of
609 the Sorokin Trough, Black Sea: Marine Geology, v. 217, p. 67–96, doi: 10.1016/j.margeo.2005.02.023.

610 Swart, P.K., 2008, Global synchronous changes in the carbon isotopic composition of carbonate sediments
611 unrelated to changes in the global carbon cycle: Proceedings of the National Academy of Sciences, v.
612 105, p. 13741–13745, doi: 10.1073/pnas.0802841105.

613 Taviani, M., Angeletti, L., Ceregato, A., Foglini, F., Froglia, C., and Trincardi, F., 2013, The Gela Basin
614 pockmark field in the strait of Sicily (Mediterranean Sea): Chemosymbiotic faunal and carbonate
615 signatures of postglacial to modern cold seepage: Biogeosciences, v. 10, p. 4653–4671, doi:
616 10.5194/bg-10-4653-2013.

617 Thiel, V., Peckmann, J., Seifert, R., Wehrung, P., Reitner, J., and Michaelis, W., 1999, Highly isotopically
618 depleted isoprenoids: molecular markers for ancient methane venting: Geochimica et Cosmochimica
619 Acta, v. 63, p. 3959–3966, doi: 10.1016/S0016-7037(99)00177-5.

620 Titschack, J., Goetz-Neunhoeffer, F., and Neubauer, J., 2011, Magnesium quantifcation in calcites [(Ca,
621 Mg)CO_3] by Retveld-based XRD analysis: Revisiting a well-established method: American
622 Mineralogist, v. 96, p. 1028–1038, doi: 10.2138/am.2011.3665.

623 Toby, B.H., 2001, EXPGUI, a graphical user interface for GSAS: Journal of Applied Crystallography, v. 34,
624 p. 210–213, doi: 10.1107/S0021889801002242.

625 Tornabene, T.G., Langworthy, T. a, Holzer, G., and Oró, J., 1979, Squalenes, phytanes and other isoprenoids
626 as major neutral lipids of methanogenic and thermoacidophilic “archaebacteria”.: Journal of molecular
627 evolution, v. 13, p. 73–83, doi: 10.1007/BF01732755.

628 ten Veen, J.H., Woodside, J.M., Zitter, T.A.C., Dumont, J.F., Mascle, J., and Volkonskaia, A., 2004,
629 Neotectonic evolution of the Anaximander Mountains at the junction of the Hellenic and Cyprus arcs:
630 Tectonophysics, v. 391, p. 35–65, doi: 10.1016/j.tecto.2004.07.007.

631 Vinçon-Laugier, A., Grossi, V., Pacton, M., Escarguel, G., and Cravo-Laureau, C., 2016, The alkyl glycerol
632 ether lipid composition of heterotrophic sulfate reducing bacteria strongly depends on growth substrate:
633 Organic Geochemistry, v. 98, p. 141–154, doi: 10.1016/j.orggeochem.2016.05.015.

634 Wiese, F., Kiel, S., Pack, A., Walliser, E.O., and Agirrezabala, L.M., 2015, The beast burrowed, the fluid

followed - Crustacean burrows as methane conduits: Marine and Petroleum Geology, v. 66, p. 631–640, doi: 10.1016/j.marpetgeo.2015.03.004.

Zhang, Y.G., Zhang, C.L., Liu, X.L., Li, L., Hinrichs, K.U., and Noakes, J.E., 2011, Methane Index: A tetraether archaeal lipid biomarker indicator for detecting the instability of marine gas hydrates: Earth and Planetary Science Letters, v. 307, p. 525–534, doi: 10.1016/j.epsl.2011.05.031.

Zitter, T. a C., Huguen, C., ten Veen, J., and Woodside, J.M., 2006, Tectonic control on mud volcanoes and fluid seeps in the Anaximander Mountains, eastern Mediterranean Sea: Geological Society of America Special Papers, v. 409, p. 615–631, doi: 10.1130/2006.2409(28).

Zwicker, J., Smrzka, D., Gier, S., Goedert, J.L., and Peckmann, J., 2015, Mineralized conduits are part of the uppermost plumbing system of Oligocene methane-seep deposits, Washington State (USA): Marine and Petroleum Geology, v. 66, p. 616–630, doi: 10.1016/j.marpetgeo.2015.05.035.

657

658

659 **Figure caption**

660 Figure 1. (A) Simplified geodynamic setting of the eastern Mediterranean Sea, showing the location of the
661 Anaximander Mountains and Athina MV (based on Aksu et al., 2009). (B) High-resolution micro-
662 bathymetric map of Athina MV acquired with AUV MARUM SEAL (Bohrmann et al., 2014), showing the
663 recent outflows and its flow directions, as well as the location of GeoB 11319-1.

664 Figure 2: ROV seafloor observations on the SW flank of Athina MV. (A) Overview of the giant colony of
665 living *Lamellibrachia anaximandri* (4-5m x 2 m top area, ca. 4 m high), sitting on an unknown structure. In
666 the background, carbonate crusts and dark bacterial mats are visible. (B) Tubeworm colonies settled between
667 decimetre-sized slab of carbonate crusts at the base of the giant colony and nearby the sampled site. (C)
668 Close view of the surface on the top of the giant colony, where tubeworms show their pinkish brachial
669 plume. (D) Oblique view at a seafloor terrace depicting dark grey TCC (highlighted in green), studied in the
670 present work.

671 Figure 3. (A) Close-up on the framework of TCC outcropping at the SW peak of Athina MV. (B) Photograph
672 of the sample GeoB11319-1 (preliminary work, Brinkmann, 2007); note the occurrence of interconnected
673 carbonate tubes.

674 Figure 4. Thin section images of one TCC from GeoB11319-1. (A) Micrograph-mosaic (cross-polarized
675 light) showing a longitudinal section through a ~2 mm wide tube; the exterior of the tube consists of Mg-
676 calcite cemented sediment (M), with scattered foraminifera and silt-sized quartz grains; the internal tube
677 surface is coated with clotted and fibrous aragonite (cfA); the interior of the tube is made up of semi-lithified
678 detrital infill (Di). (B) and (C) are magnifications (plane-polarized light) of the tube-wall, highlighting dark-
679 grey spots produced by Feigl's staining of cfA.

680 Figure 5. Stable isotopic composition ($\delta^{13}C$ and $\delta^{18}O$) from different phases of the TCC. Abbreviations: cfA,
681 clotted and fibrous aragonite; M, high-Mg calcitic micrite; Di, detrital infilling.

Figure 6. A) GC-MS total ion current chromatogram of alcohols as TMS-derivatives extracted from subsample A. Displayed $\delta^{13}C$ values (in ‰) of selected biomarkers given are related to AOM (green) or algal input (red). B) Base peak HPLC-MS chromatogram of characteristic GDGTs in the TLE aliquot obtained from subsample A. Numbers indicate the number of cyclopentane rings within GDGTs, including ring (GDGT-2a and 2) and stereo (GDGT-5 and 5') isomers (Becker et al., 2013).

Figure 7. Occurrence and classification of the TCC in the present-day oceans and in the fossil sedimentary record. The numbers in each site in the figure refer to the key references in Appendix I (Suppl. Mat.).

Figure 8. Sketch of the formation hypotheses for the TCC at Athina MV: (A) tubeworm fossil hypothesis (based on (Dattagupta et al., 2008), with the observed aragonitic laminations and chitinic tube wall characterizing the mineralization of the sediment-immersed portion of the tubeworms (Haas et al., 2009). (B) Lithified burrows hypothesis (based on Zwicker et al., 2015), with altered minerals at the internal surface (like Fig. 4) of the conduits as potential result of the exposure to the seafloor waters, marking the interruption of methane-rich fluids seepage through the TCC.

705

706

707 **Tables**

708 Table 1: Mineralogical compositions of the tubular conduit. MgC = Magnesian calcite; Kte = kutnahorite
709 Mn-carbonate; CaC= low Mg-calcite; Ara = Aragonite; Qtz = Quartz; Fsp = Feldspars; Clays = clay
710 minerals. Quantitative weight fraction: major > 20 %; 5% < minor < 20%; trace < 5%. Further details are
711 provided in the Suppl. Mat.

Subsample	Lithology	Major	Minor	Trace	Mg (mol %) content in MgC
A1	Detrital infilling	MgC	Kte, CaC	Ara, Qtz,	10.1(±0.7)
B1	Micrite	MgC, Kte	CaC	Ara, Qtz	20.9 (±1.2)
F1	Micrite	MgC	Kte, CaC	Ara, Qtz	11.1 (±1.6)
F2	Micrite	MgC	Kte, CaC, Ara	Qtz	15.3 (±0.8)
F3	Micrite	MgC	Kte, CaC	Ara, Qtz, Clays	17.9 (±1.0)
0-A1	Detrital infilling	MgC, CaC	Qtz, Clays	Fsp, Kte	5.2 (±2.2)
0-A2	Micrite	MgC	Kte. Ara, CaC	Qtz	17.1 (± 0.7)
0-A3	Micrite	MgC	Kte. Ara, CaC	Qtz. Clays	14.8 (± 1.0)
0-A4	Micrite	MgC, Ara	Kt, CaC	Qtz, Clays	12.2 (± 0.9)
0-A5	Micrite	MgC, Kte	Ara, CaC	Qtz	15.6 (±1.2)
0-A6	Micrite	MgC	CaC, Ara	Qtz, Kte, Clays	11.8 (±1.1)

712

713

714

715

716 Table 2: Compound-specific $\delta^{13}C$ values and putative sources of selected lipid biomarkers and MI of the two
717 subsamples analysed. PMI = 2,6,10,15,19-pentamethylicosane; Bp = biphytane; Bp-Cren = biphytane
718 derived from crenarchaeol, DAGE= dialkyl glycerol ether, FA = fatty acid, ai = methyl-branching at ante-iso
719 position (ω3).

	Compounds	**$\delta^{13}C$ (‰ V-PDB)**		**Putative sources**
		A	**B**	
	Phytane	−32.2	−31.5	Chlorophyll degradation, archaeal input
	PMI	−40.2	−49.3	Methanogens, anaerobic methanotrophs
	C_{27}	−29.6	−30.4	Terrestrial input
GDGT-derived	Bp- 0	−61.2	−54.4	Anaerobic methanotrophs, planktonic archaea
GDGT-derived	Bp-1	−60.4	−58.4	Anaerobic methanotrophs, planktonic archaea
GDGT-derived	Bp-2	−30.7	−30.4	Anaerobic methanotrophs, planktonic archaea
GDGT-derived	Bp-Cren	−22.3	−20.2	Planktonic archaea
	Cholesterol	−28.6	−26.9	Algal input
	DAGE C_{30} (*ai*-$C_{15:0}$/*ai*-$C_{15:0}$)	−78.5	−65.1	Bacteria associated with AOM, incl. autotrophic and heterotrophic SRB
	Archaeol	−89.8	−84.0	Anaerobic methanotrophs
	FA *ai*-$C_{15:0}$	−29.9	−32.2	Anaerobic bacteria incl. SRB
	MI	0.58	0.52	

720

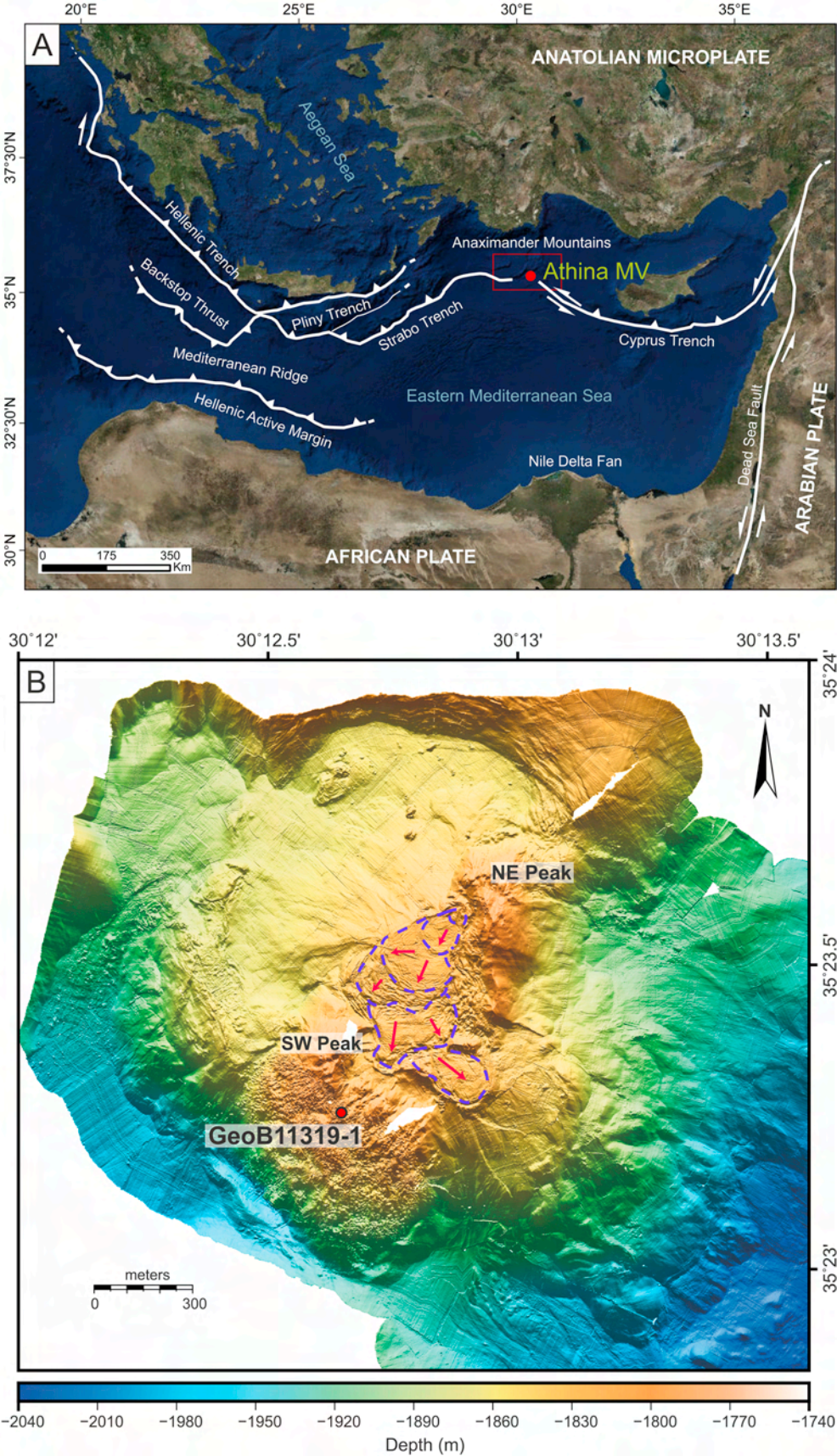
A
20°E
25°E
30°E
35°E
37°30'N
35°N
32°30'N
30°N
ANATOLIAN MICROPLATE
Aegean Sea
Hellenic Trench
Backstop Thrust
Pliny Trench
Strabo Trench
Anaximander Mountains
Athina MV
Cyprus Trench
Mediterranean Ridge
Hellenic Active Margin
Eastern Mediterranean Sea
Nile Delta Fan
Dead Sea Fault
ARABIAN PLATE
AFRICAN PLATE
0 175 350 Km
B
30°12'
30°12.5'
30°13'
30°13.5'
35°24'
35°23.5'
35°23'
N
NE Peak
SW Peak
GeoB11319-1
meters
0 300
−2040 −2010 −1980 −1950 −1920 −1890 −1860 −1830 −1800 −1770 −1740
Depth (m)

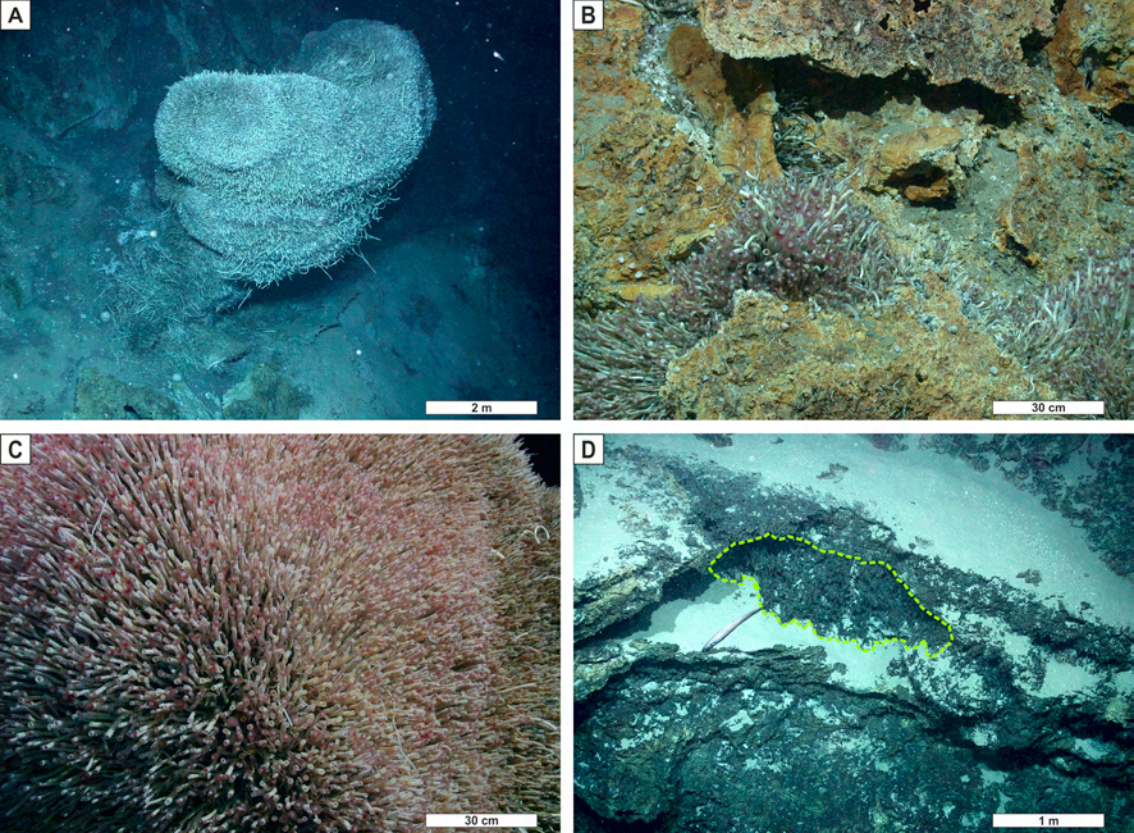
A
2 m
B
30 cm
C
30 cm
D
1 m


A
30 cm

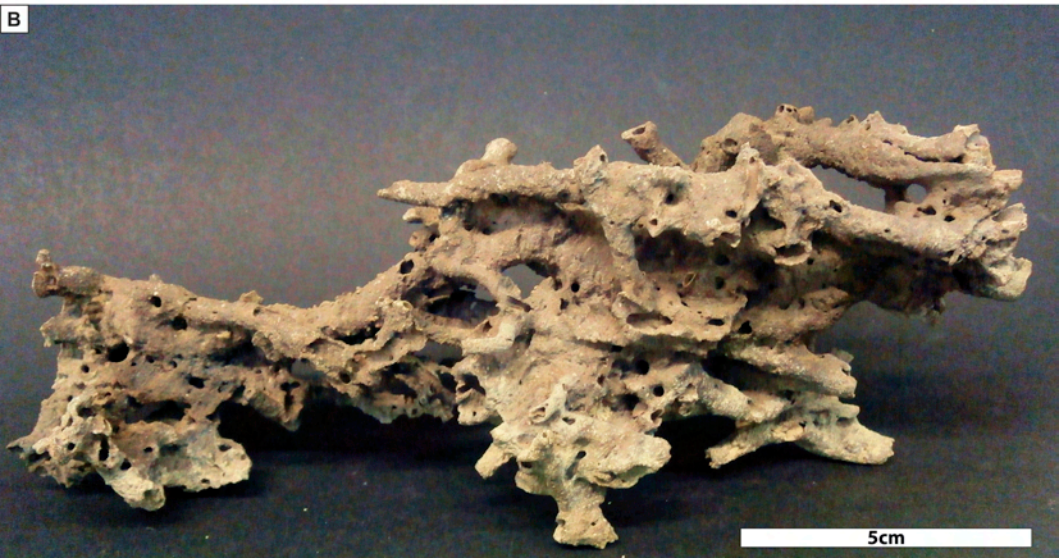
B
5cm

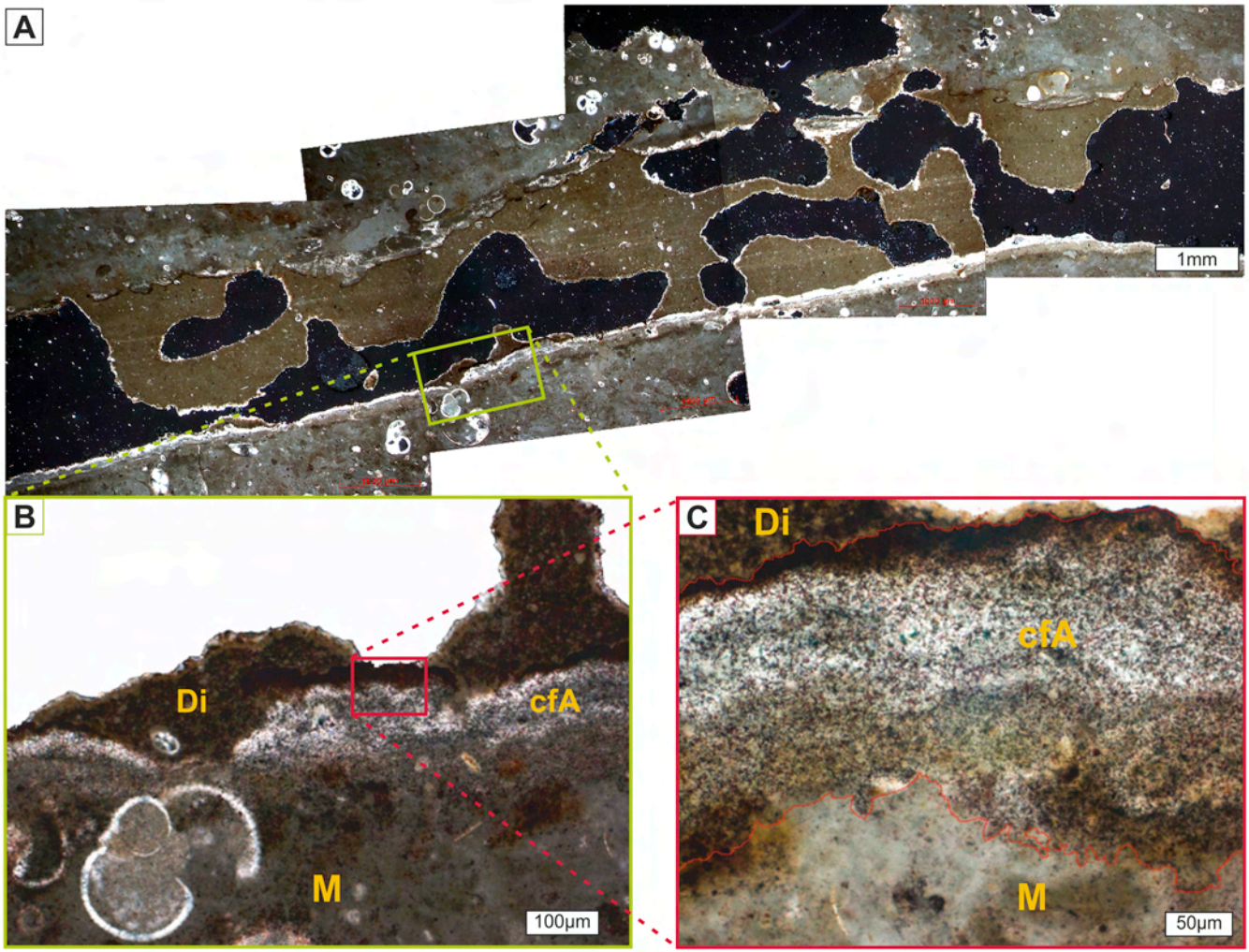
A
1mm
B
Di
cfA
M
100µm
C
Di
cfA
M
50µm

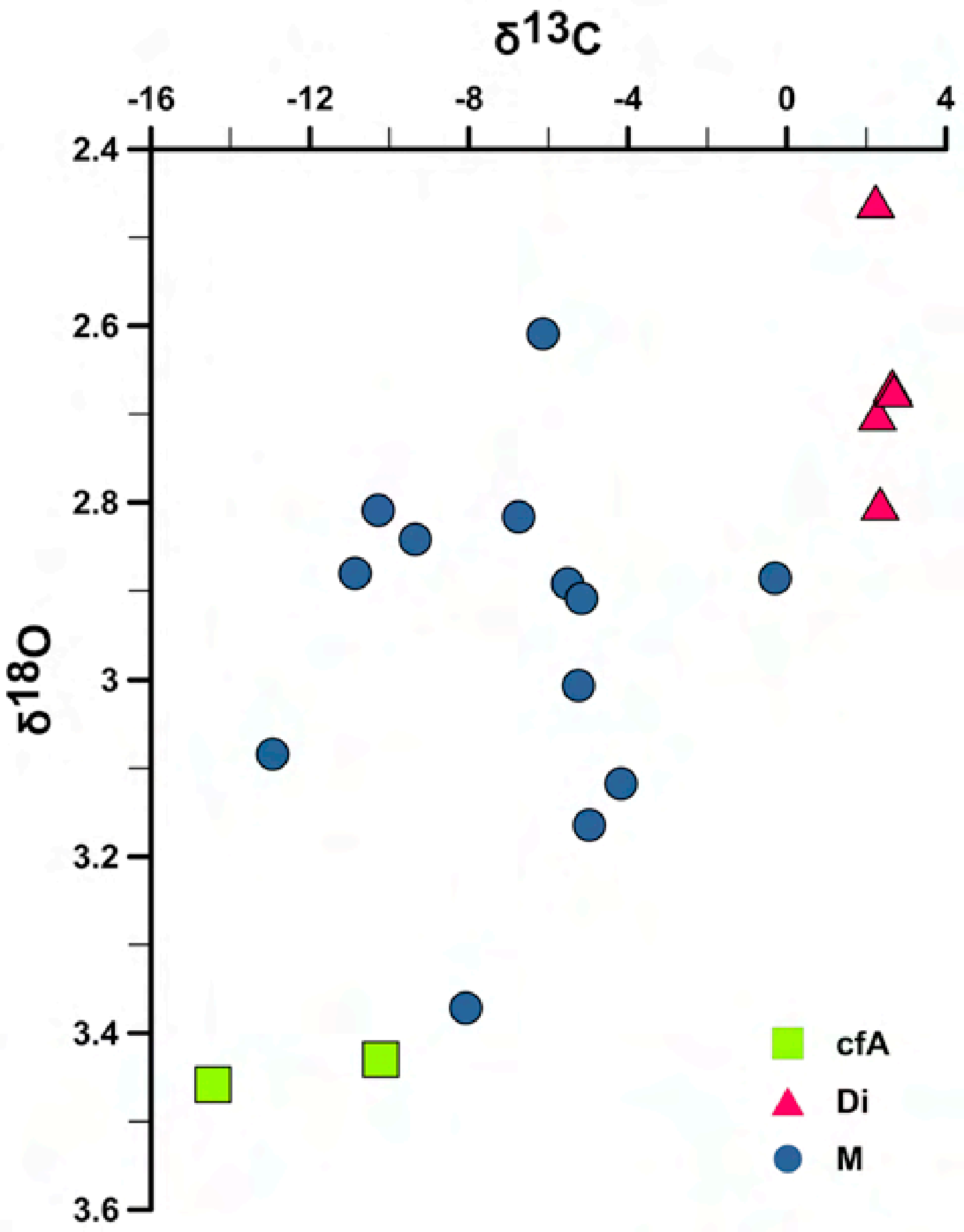
δ13C
-16
-12
-8
-4
0
4
2.4
2.6
2.8
3
3.2
3.4
3.6
δ18O
cfA
Di
M

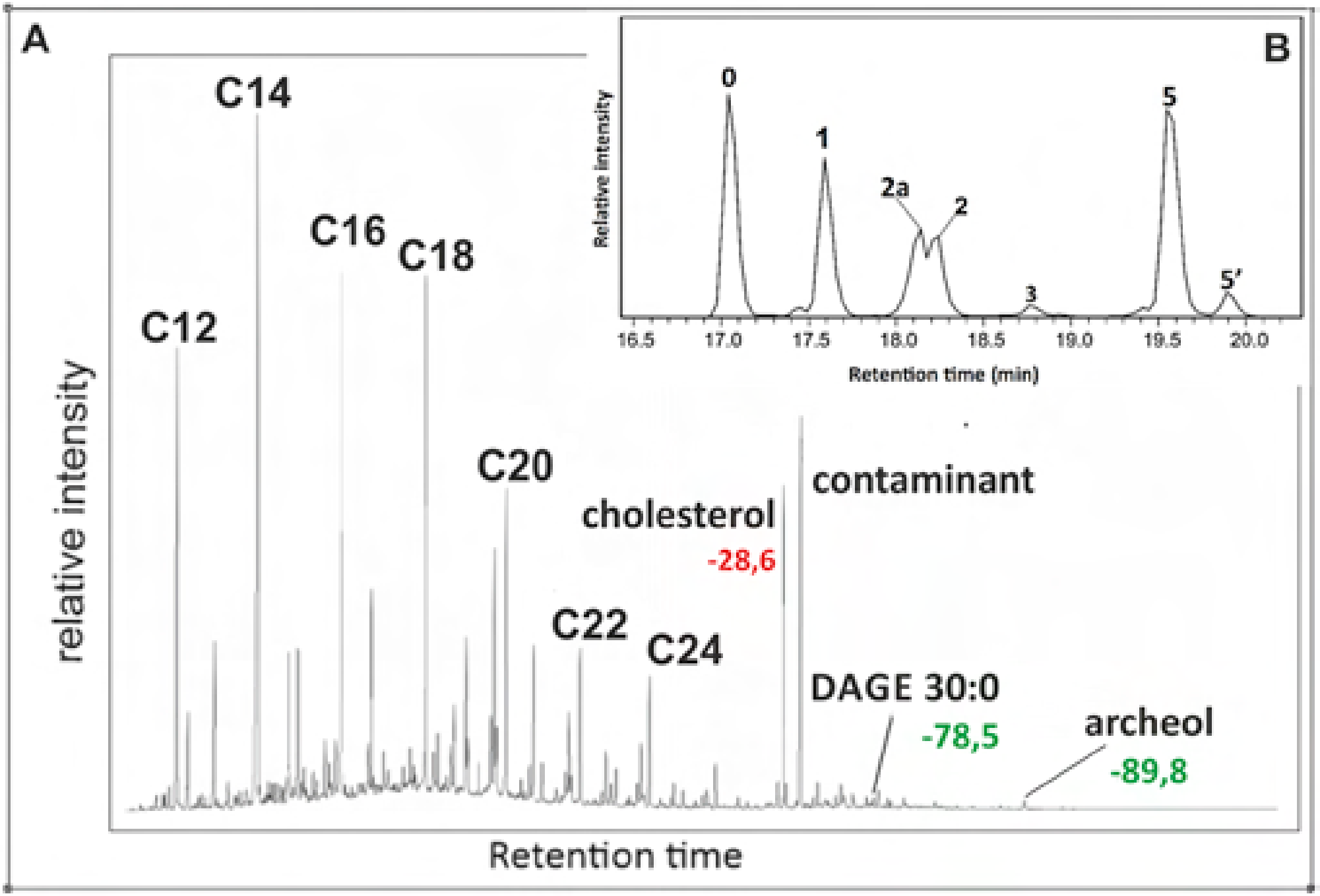
A
B
C14
C16
C18
C12
C20
C22
C24
cholesterol
-28,6
contaminant
DAGE 30:0
-78,5
archeol
-89,8
relative intensity
Retention time
Relative intensity
0
1
2a
2
3
5
5'
16.5
17.0
17.5
18.0
18.5
19.0
19.5
20.0
Retention time (min)

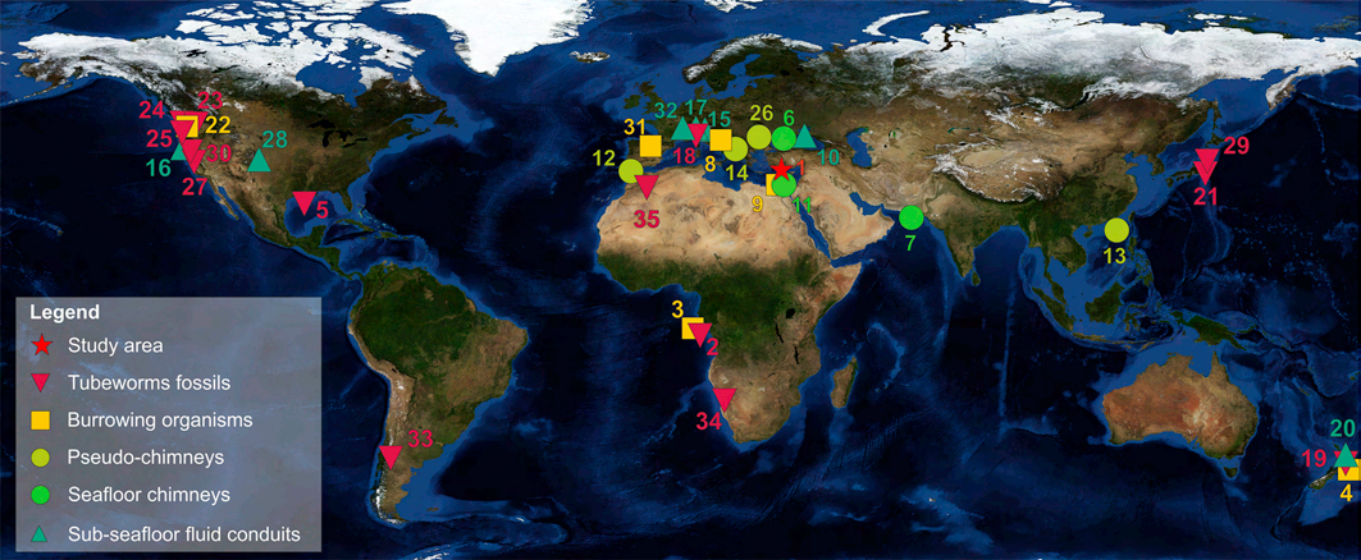
Legend
Study area
Tubeworms fossils
Burrowing organisms
Pseudo-chimneys
Seafloor chimneys
Sub-seafloor fluid conduits
1
2
3
4
5
6
7
8
9
10
11
12
13
14
15
16
17
18
19
20
21
22
23
24
25
26
27
28
29
30
31
32
33
34
35

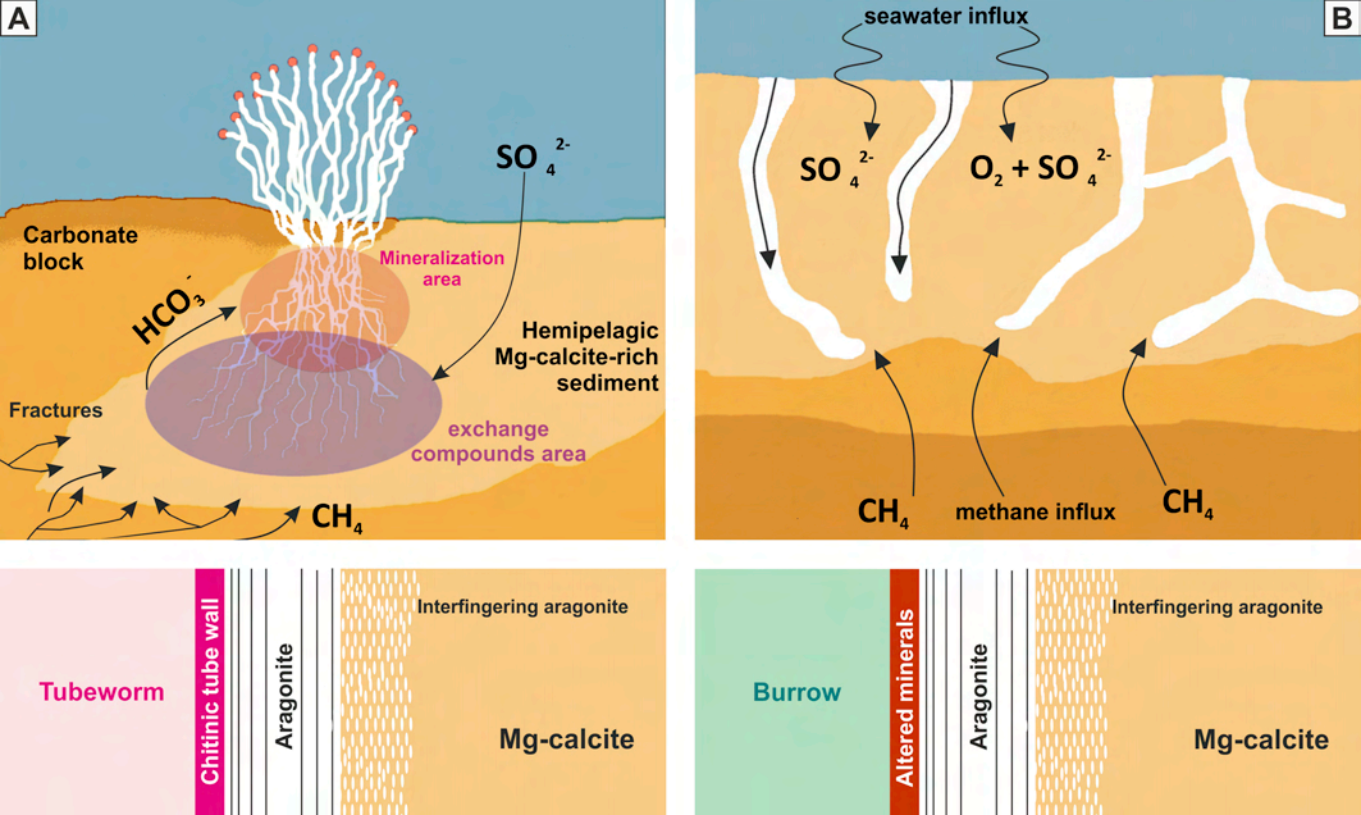
A
SO_4^{2-}
Carbonate block
Mineralization area
HCO_3^-
Hemipelagic Mg-calcite-rich sediment
Fractures
exchange compounds area
CH_4
B
seawater influx
SO_4^{2-}
$O_2 + SO_4^{2-}$
CH_4
methane influx
CH_4
Tubeworm
Chitinic tube wall
Aragonite
Interfingering aragonite
Mg-calcite
Burrow
Altered minerals
Aragonite
Interfingering aragonite
Mg-calcite